PCCP

Accepted Manuscript

ROYAL SOCIETY OF CHEMISTRY

www.rsc.org/pccp

Modification Mechanism of Praseodymium Doping for the Photocatalytic Performance of TiO_2: A Combined Experimental and Theoretical Study

Zhi-Gang Duan[1,2], Zong-Yan Zhao[1,*], Qing-Nan Shi[1]

[1] Faculty of Materials Science and Engineering, Key Laboratory of Advanced Materials of Yunnan Province, Kunming University of Science and Technology, Kunming 650093, People's Republic of China

[2] College of Science, Southwest Forestry University, Kunming 650224, People's Republic of China

[*]Corresponding author, E-mail: zzy@kmust.edu.cn. Tel: +86-871-65109952, Fax: +86-871-65107922.

Abstract

Impurity doping is a simple and efficient modification method to improve the photocatalytic performance of wide band gap photocatalyst. However, some basic and important issues about the mechanism of impurity doping modification still need to be further confirmed and explained. In the present work, Pr-doped TiO_2 with mono-phase crystal structure is adopted as the research object, and prepared by Sol-Gel method. Then, the crystal structure, binding information, optical absorption, and photocatalytic activity have been systematically investigated. The experimental results shown that Pr doping could obviously enhance the photocatalytic activity of TiO_2, and the modification effects for rutile TiO_2 is more obvious than for anatase TiO_2. In order to understand the underlying mechanism, density function theory is utilized to calculate the crystal structure and electronic structure of pure and Pr-doped TiO_2. The differences of electronic structure between anatase and rutile phases lead to above photocatalytic performance. The experimental measurements and theoretical calculations can confirm and explain each other in the present work. And two points are confirmed: the position of band edge determines the redox activity of photocatalyst, and the shallow energy bands induced by impurity doping could improve the photocatalytic performance.

Keywords

Photocatalysis; Titanium dioxide; Pr doping; DFT calculations

1. Introduction

Photocatalysis technology is attracting more and more concerns, because it could converse solar energy into chemical energy to solve the issues of energy shortage and environmental pollution: producing hydrogen by photocatalytic water splitting, converting CO_2 to hydrocarbon fuels or decomposing organic pollutant by photocatalytic reactions.[1-4] However, the development of photocatalysis technology suffers from narrow spectral response range for sunlight or low quantum conversion efficiency for solar energy. Nowadays, the researches are concentrating on the following two aspects: development of novel photocatalyst or photocatalytic system (for example, 2D layered compounds, metal-free polymeric photocatalyst),[5, 6] and modification of traditional photocatalyst (such as TiO_2, ZnO, Fe_2O_3, etc.). TiO_2-based photocatalyst is still received considerable attention, due to its various advantages: multi-function, non-toxic, long-term stability, low-cost.[7-10] Moreover, it always acts as the typical representative and the prototype for photocatalyst. However, as a wide band gap semiconductor (3.2 eV for anatase, 3.0 eV for rutile), it is only activated by UV-light irradiation, whose energy only account for about 4% of the whole solar energy, because the electron excitation requires incident photon energy must larger than the band gap energy.[11, 12] To obtain a more efficient utilization of solar energy for TiO_2-based photocatalyst, researchers adopted various modification methods (including: impurity doping,[13-15] cocatalyst loading,[16, 17] dye-sensitizing,[18, 19] semiconductor compositing,[20-22] and so on), to improve the photocatalytic performance of TiO_2 under visible-light irradiation.

Among these modification methods, impurity doping is easy and simply carried out, and its modification effects are obvious, attracting extensive concerns. First, impurity doping could form impurity states in the forbidden band, which not only can make the electrons are excited by visible-light, but also can capture photo-generated electrons or holes, reducing recombination probability of photo-generated electron-hole pairs or prolonging lifetime of photo-generated carrier.[9, 23, 24] For the extension of TiO_2 photocatalytic activity in the visible range of the electromagnetic spectrum, the presence of impurity states in the forbidden band is very important: the lower energy photon could excite electron from valence band to these impurity states, and then another lower energy photon could excite them to the conduction band. By this relay excitation, TiO_2 could show photocatalytic performance under visible-light irradiation. Second, impurity doping could change the local crystal structure to produce local crystal distortion and the electrons distribution. Thus, the centers of positive charges and negative charges are not longer coincided

together, which can produce the local internal electric field. Owing to the directions of electric force on electrons and holes are just opposite, so this local internal electric field could further promote the separation of photo-generated electron-hole pairs.[8] For impurity doping, the basic requirements are: producing impurity energy states in the band gap, processing higher energy levels than the H_2/H_2O level, and having impurity energy states sufficiently overlapping with conduction band or valence band.[25] After years of extensive investigation, the impurity doping modification for TiO_2 made considerable progress: transition-metal mono-doping,[26, 27] non-metal mono-doping,[8, 28, 29] different impurities co-doping,[30-32] both in experimental and theoretical investigations. These progresses deepen the fundamental understand the modification mechanism of impurity doping, and establish the foundation for the further development of photocatalysis technology.

However, some open questions remain unsolved in above mentioned research progress: (i) the underlying mechanism of impurity doping modification is not completely clear, especially the relationships with crystal structure and electronic structure; (ii) impurity doping maybe make TiO_2 to absorb visible-light, but sometimes reduces the redox activity at the same time; (iii) some conclusions in different literatures are inconsistent, owing to different synthesis route or different evaluate criteria. In published reports, Huang et al. prepared Pr-TiO_2 photocatalyst samples by Sol-Gel method, and found that praseodymium doping could bring about remarkable improvement in the photoactivity under UV-light irradiation, which high activity was attributed to produce the lattice distortion and inhibit efficiently of the recombination of the electron-hole by Pr^{3+};[33] and Wu et al. synthesized Pr+N co-doped TiO_2 nanoparticles by sol-gel method combined with microwave chemical method, and observed that synergistic effect between Pr and N to remarkable improve the photocatalytic activity of TiO_2.[34] Because of the unique 4f electron configuration and spectrum properties, rare earth ions are ideal dopant for modifying the crystal structure, electronic structure, optical properties and surface absorption of TiO_2 and forming some novel promising photocatalysts.[35, 36] In the field of photocatalysis, rare earth ions dopant could provide the adequate and matched energy states with the host energy band, meaning have more opportunity to meet the advantages of impurity doping effects. In our previous work, we found that Pr-doping could form impurity energy states below the bottom of conduction band of TiO_2, which meets the basic requirements of impurity doping as mentioned above.[36] But this work did not consider the spin-orbital coupling effects that is very important for rare earth elements, and only studied the doping effects in anatase TiO_2. Based on above reasons, we choice praseodymium as dopant to improve the photocatalytic performance of TiO_2, in order to preliminary

solve these open problems. In other words, the initial purpose of this article is to in-depth exploring the underlying modification mechanism of praseodymium doping for TiO_2 in different crystal structures. In the present work, we first synthesize and characterize Pr-doped TiO_2 samples, and then further adopted density functional theory (DFT) with GGA+U method to calculate and compare the doping effects of Pr in anatase and rutile TiO_2. Combing with experimental observation and theoretical calculations, the detailed modification mechanism of Pr for TiO_2 will be discussed, and provide an example for the research for photocatalysis technology.

2. Experimental and computational methods

A. Materials. Tetrabutyl titanate [$Ti(OC_4H_9)_4$] (98%, Aldrich), Praseodymium nitrate [$Pr(NO_3)_3.6(H_2O)$] (99%, Aldrich), Concentrated nitric acid [HNO_3] (99%, Aldrich), and Anhydrous alcohol [C_2H_5OH] were all of analytical grade and used without further purification. Deionized water was obtained fromlaboratory purification system.

B. Preparation of Samples. The Pr-doped TiO_2 samples were synthesized by a conventional process, sol-gel method. Firstly, 5 ml of $Ti(OC_4H_9)_4$ was added dropwise in 100 ml of anhydrous alcohol, under constant magnetic stirring at room temperature, obtaining yellow transparent solution (denoted "A" solution). Secondly, a mixture of 10 ml of anhydrous alcohol and 1.5 ml deionic water (denoted "B" solution) was slowly added dropwise into "A" solution. Then, the "A+B" mixed solution was hydrolyzed at room temperature, under vigorous magnetic stirring for 2 hours, obtaining pale yellow transparent sol. During this process, the pH value is maintained at 3 by adjustment of dilute nitric acid. Then, the sol was aged for 4 days at room temperature to prepare gel, and the derived gel was dried at 80 □ for 24 hours to remove the solvents. Finally, the dry gel was carefully ground into powder, and annealed at different temperatures of 500 □ (for samples with anatase phase) and 950 □ (for samples with rutile phase) in the muffle furnace in the air for 3 hours to obtain desired pure TiO_2 samples. The Pr-doped TiO_2 samples were synthesized with the same method mentioned above, except for the addition of praseodymium nitrate solution into the "B" solution. The doping concentrations were keep for the mol fraction (Pr/(Ti+Pr) = 0.5 mol%).

C. Characterization of Samples. The structure of the as-prepared sample were identified by X-ray diffractometer (XRD, Cu-Kα: λ = 1.542 Å, D8 Advance, German), where the diffracted X-ray intensities

were recorded as a function of 2θ. The accelerating voltage was 35 kV and the applied current was 25 mA, and the sample was scanned from 10° to 90° (2θ) in steps of 0.02°. X-ray photoelectron spectroscopy (XPS, Escalab 250, USA) measurement was carried out to analyze the valence state of compositions. The binding energies of all investigated elements were calibrated with the C1s peak at 284.6 eV for the adventitious carbon. The target power was run at 280 W and the accelerating voltage was kept at 13.5 KV. The optical properties of absorption were measured by ultraviolet-visible diffuse reflectance spectra of the sample were recorded with a Shimadzu UV-2401 PC spectrophotometer equipped with an integrating sphere using $BaSO_4$ as the reference standard at room temperature in air.

D. Photocatalytic performance evaluation. Methylene blue (MB) degradation technique was employed for investigating the photocatalytic activity of pure and Pr-doped TiO_2 in aqueous solution under simulated sunlight. A common fluorescent lamp (30 W, spectral range: 350-750 nm) is chosen as solar simulator. In a typical photocatalytic degradation experiment, 50 ml of an aqueous solution of 10 mg/L MB solution was continuous magnetic stirring well with 0.20 g of samples powders in a 100 mL glass beaker. Before irradiation, the suspension was equilibrated in the glass beaker by stirring in the dark for one hour to equilibrate the adsorption of MB onto the surface of samples. An air cooler and thermostat were connected to the solar simulator to maintain the temperature of suspension at in-door temperature (~25 ℃). Aliquots (4 mL) were withdrawn from the suspension under simulated sunlight irradiation at regular irradiation interval of one hour. These aliquots were centrifuged at 3500 rpm for 40 minutes to separate the photocatalyst from the mixture. The absorption spectra were recorded using JH722N UV-Vis spectrophotometer, in which the absorption constant at 664 nm of the MB aqueous was measured to determine the MB concentration. The photocatalytic degradation constant of MB in the solution was calculated by the following formula: $D = \left[\frac{C_0 - C}{C_0}\right] \times 100\%$, where C_0 is the initial concentration of MB after one hour dark stirring, and C is the concentration of MB after a time *t*.

E. DFT calculations. In the present work, all of the calculations were carried out by using the periodic density functional theory package of Cambridge Serial Total Energy Package (CASTEP) codes.[37] The core electrons (Ti: [Ar], O: [He], Pr: [Xe]) were treated with the ultrasoft pseudopotential. The exchange-correlation effects of valence electrons (Ti: $3d^2 4s^2 6p^3$, O: $2s^2 2p^4$, Pr: $4f^3 5d^0 6s^2$) were described by the revised Perdew-Burke-Ernzerhof for solid (PBEsol) of generalized gradient approximation (GGA).[38] In order to obtain accurate electronic structure, the method of GGA+U was adopted to overcome the

well-known shortcoming of GGA [39]. The U value of 4.2 eV was applied to the Ti-d states, Pr-f states, and the O-p states. Using these values, the accurate band gaps could be obtained that could be compared with experimental measurements, as well as keeping the main features of electronic structure obtained by the standard DFT calculations. The Monkhorst-Pack scheme K-points grid sampling was set as 4×4×2 for the irreducible Brillouin zone. A 60×60×80 mesh was used for fast Fourier transformation. An energy cutoff of 380 eV was used for expanding the Kohn-Sham wave functions. The minimization algorithm was chosen the Broyden-Fletcher-Goldfarb-Shanno (BFGS) scheme [40]. Its convergence criteria were set as follows: the force on the atoms were less than 0.03 eV/Å, the stress on the atoms were less than 0.05 GPa, the atomic displacement was less than 1×10^{-3} Å, and the energy change per atom was lower than 1×10^{-5} eV. A 3×3×2 supercell (for anatase phase) and 2×2×3 supercell (for rutile phase) were used for constructing the Pr-doped TiO_2 models, in which a Ti atom in the supercells was replaced by a Pr atom. In the supercells, the total number of atoms is reached to 108 (for anatase phase) or 72 (for rutile phase).

3. Results and discussions

3.1 Crystal structure of pure and Pr-doped TiO_2.

FIG. 1 shows the X-ray diffraction (XRD) patterns of the pure and Pr-doped TiO_2 samples. All the peaks can be exclusively indexed on the basis of the anatase phase of TiO_2 (JCPDS No. 21-1272, space group $I4_1/amd$) or rutile phase of TiO_2 (JCPDS No. 21-1276, space group $P4_2/mnm$), respectively. This result indicates that all samples exhibit well crystallized mono-phase (anatase or rutile phase). No other peaks corresponding to Pr metal or related compounds are observed in Pr-doped TiO_2. As showed in FIG. 1, the position of main diffraction peaks are no appreciable variation or shifting, suggesting that the lattice distortion induced by Pr doping is very slight. Actually, the stability of RE-doped TiO_2 is depended on the doping level, and the doping level is very small (0.5 mol%) in the present work. So, the Pr-doped TiO_2 present stable in the annealing temperature range. Furthermore, the main diffraction peaks of Pr-doped anatase TiO_2 is weakening and broadening in compared with the corresponding pure anatase TiO_2; while the main diffraction peaks of Pr-doped rutile TiO_2 is keeping the features of sharp and strong as pure rutile TiO_2. According to Scherrer Equation, Pr doping may reduce the crystallinity of anatase TiO_2, and has no obvious influence for the crystallinity of rutile TiO_2, under present preparation conditions. The particle size of samples is another important factor to determine photocatalytic performance, especially at the nano-scale.

So, in the present work, we try our best to keep the particle size at the comparable order as possible. As shown in FIG. S1 of Electronic Supplementary Information, the average particle size of samples is listed as following: 45.31 ± 5.41 nm for pure anatase TiO_2; 68.43 ± 7.10 nm for Pr-doped anatase TiO_2; 67.38 ± 2.24 nm for pure rutile TiO_2; 56.41 ± 3.65 nm for Pr-doped rutile TiO_2. These comparable particle sizes imply that the particle size effect could be ignored in the present work.

XPS measurements of the Pr-doped TiO_2 were performed to obtain the information of the oxidation state of Pr impurity in TiO_2 host lattice. The survey and high-resolution XPS spectra of 0.5 mol% Pr-doped TiO_2 samples are illustrated in FIG. 2, which are compared with pure TiO_2. The four survey spectra have the similar curves, revealing that there has not any change for the chemical valence of Pr ions both in anatase and rutile phases (FIG. 2(a)). Such conclusion can also be supported by the high-resolution spectra of Ti-2p as well as Pr-3d in FIG. 2(b) and FIG. 2(c). The binding energy of the Pr-$3d_{5/2}$ and Pr-$3d_{3/2}$ appeared at ~932 and ~952 eV correspond to the energy of Pr^{3+} photoelectrons; the Ti-2p spectra shown at ~460 and ~465 eV assign to the binding energies of Ti-$2p_{3/2}$ and Ti-$2p_{1/2}$ for Ti^{4+} ions, respectively [41-43]. Except the slight displacements, the position and shape of Ti-2p peaks in Pr-doped TiO_2 are similar with the corresponding peaks in pure TiO_2, indicating that Pr doping does not change the chemical valence states of Ti. On the other hand, the differences of Pr-3d peaks between in anatase and rutile phases suggest that the Pr^{3+} cations have different local chemical environment at different crystal phases (anatase or rutile).

3.2 Optical properties and photocatalytic performance of pure and Pr-doped TiO_2.

UV-Vis absorption spectra of pure and Pr-doped TiO_2 samples are showed in FIG. 3. For pure TiO_2 samples, the strong absorption band at low wavelength near ~400 nm for pure anatase TiO_2, or ~420 nm for rutile pure TiO_2, indicating the presence of Ti species as tetrahedral Ti(IV). The fundamental absorption edge of pure and Pr-doped anatase TiO_2 samples are located about 390 nm; while those of rutile and Pr-doped TiO_2 samples are located 410 nm. The absorption edge slightly extends to shorter wavelengths for Pr-doped TiO_2 samples, and absorption tail in the visible-light region over 440-520 nm and strong absorption band in the UV-light region is clearly observed. It is well known that the impurity doping could impact the electronic structure of host, namely the band gap energy. For Pr-doped TiO_2 samples both with anatase and rutile phases, their fundamental absorption edges are slightly blue-shifting. However, the blue-shifts are too slight, which are coinciding with those of pure TiO_2. These observations indicate that Pr

doping could not obviously change the band gaps of TiO_2 both with anatase and rutile phases. In addition, in the range of 440-520 nm and 570-620 nm, there are two absorption bands that only observed in Pr-doped TiO_2 samples, and they could be assigned to the electron transitions of $^3H_4 \rightarrow {}^3P_2$ (455 nm), $^1I_6$ (466 nm),$^3P_1$ (479.5 nm), $^3P_0$ (496 nm), and $^1D_2$ (603.5 nm) of Pr^{3+} by visible-light excitation. If the Pr doping content increasing, these absorption peaks will be more obvious, as shown in FIG. S2 in Electronic Supplementary Information. However, for the Pr doping with 0.5% content, these absorption peaks are too weak to impact the optical properties of TiO_2. Thus, it is could be considered that the following improvement of photocatalytic performance caused by variation of optical absorption can be neglected.

The methylene blue (MB) photocatalytic degradation by pure and Pr-doped TiO_2 under simulated sunlight irradiation is presented in FIG. 4. After one hour fully stirring under dark conditions, MB reaches the equilibrium between adsorption and desorption at the samples' surfaces. The concentration of MB is decreasing from 10 mg/L to ~8.25-8.38 mg/L, meaning that all the samples have the similar absorption capacity for MB and the size or pore effects could be ignored in the present work. After five hours photocatalytic degradation, the concentration of MB is gradually decreasing to: 3.58 mg/L on pure anatase TiO_2, 2.83 mg/L on Pr-doped anatase TiO_2, 6.45 mg/L on pure rutile TiO_2, and 5.56 mg/L on Pr-doped rutile TiO_2, respectively. Compared with the initial concentration at the beginning of light on, the corresponding photocatalytic degradation degree of these samples is 57.01%, 65.66%, 23.03%, and 33.54%, respectively. These results clearly indicate that: the photocatalytic activity of anatase TiO_2 is higher than that of rutile TiO_2; and Pr doping could obviously improve the photocatalytic activity of TiO_2 under simulated sunlight irradiation.

In order to further analyze the reaction kinetics, the photocatalytic degradation data were fitted, which fitting equations and curves are presented in FIG. 4. The results showed that the process of photocatalytic degradation of MB on TiO_2 follows the first order reaction kinetics model: the apparent first order activation constant is linear to reaction time:

$$-\frac{dC}{dt} = kC \ \ or \ \ C = C'\exp(-kt) + C_L \quad \text{(Eq. 1)}$$

$$-\frac{dD}{dt} = kD \ \ or \ \ D = D'\exp(-kt) + D_L \quad \text{(Eq. 2)}$$

where C' or D' represents the pre-exponential factor, k represents the chemical reaction rate constant, and the C_L or D_L represents the limiting concentration or limiting degradation rate. The C_L or D_L indicates the final limitation when the time tends to infinity. As the fitting curves shown, the reaction rate constant and

limiting concentration (or limiting degradation rate) of anatase TiO_2 is higher than that of rutile TiO_2, and Pr doping could enhance these reaction parameters. On the other hand, there are still differences between anatase and rutile cases. By Pr doping, the reaction rate constant of anatase TiO_2 is increasing by 0.014 h^{-1}, and the limiting degradation rate is increasing by 9.07%; while the reaction rate constant of rutile TiO_2 is increasing by 0.03 h^{-1}, and the limiting degradation rate is increasing by 12.17%. These results suggest that the modification effects of Pr doping is more obvious for rutile TiO_2 than that for anatase TiO_2.

3.3 Electronic structure of pure and Pr-doped TiO_2.

To better understand the above experimental results for Pr-doped TiO_2 photocatalysts, we further adopted the DFT method to investigate the underlying mechanism. In the case of pure anatase TiO_2, the calculated lattice parameters are listed as following: a = b = 3.7739 Å, c = 9.5822 Å. And in the case of pure rutile TiO_2, the calculated lattice parameters are listed as following: a = b = 4.5958 Å, c = 2.9457 Å. These calculated lattice parameters are consistent with the experimental measurements,[44] suggesting that the calculation method adopted in the previous work is reliable. Since the different valence states and ionic radius, Pr doping will distort TiO_2 crystal lattice. As shown in TABLE 1, Pr-O bond length is larger than Ti-O bond length, and thus the volume of crystal cell of Pr-doped TiO_2 is slightly increasing. In the case of Pr-doped anatase TiO_2, the calculated lattice parameters are listed as following: a = b = 3.7800 Å, c = 9.6392 Å. And in the case of Pr-doped rutile TiO_2, the calculated lattice parameters are listed as following: a = b = 4.6616 Å, c = 2.9725 Å. Compared with the lattice parameters of pure TiO_2, we found that the lattice distortion caused by Pr ions doping is very slight. In the XRD measurement (as shown in FIG. 1), the main patterns did not occur significant offset, which suggest the experimental measurements and theoretical calculations can confirm each other in the present work.

To examine the relative difficulty for Pr impurity to incorporate into different host lattice sites, the impurity formation energies (E_f) are then discussed. The formation energy was calculated according to the formula that is defined by Van de walle et al.[45] The smaller the E_f value means that the corresponding doping process could be easier carried out. In the present work, we found that the E_f value of Pr-doped anatase TiO_2 is smaller than that of Pr-doped rutile TiO_2, which indicates that Pr doping into anatase phase is easier than rutile phase. And in the experimental section, the annealing temperature of Pr-doped anatase TiO_2 sample is smaller than that of Pr-doped rutile TiO_2 sample, which could partly explained by this

calculated result. Furthermore, as shown in TABLE 1, the atomic or bond populations (namely charge distribution) are decreasing by Pr doping, except the bond population of longer Ti-O bonds. The changes of bond length, crystal volume, and atomic or bond populations will lead to local lattice deformation, and resulting in forming the build-in inner local electric field. This is efficient effect to enhance the photocatalytic activity of TiO_2.

The calculated band structures are illustrated in FIG. 5, with the corresponding density of states. The band gap energy (between the valence band maximum, VBM, and the conduction band minimum, CBM) of pure anatase and rutile TiO_2 are 3.196 and 2.996 eV, respectively, which are in agreement with experimental measurements. And the band gap energy of Pr-doped anatase and rutile TiO_2 are 3.130 and 2.991 eV, respectively. Compared these results, we found that the Pr ions doping could slightly reduce the band gap of TiO_2. However, these differences are too small to distinguish. These calculated results confirmed the measurement observations of UV-Vis diffuse reflectance spectroscopy as shown in FIG. 3. In the case of Pr-doped anatase TiO_2, there are two impurity energy levels above the valence band with a distance of 0.358 eV from the VBM (with a bandwidth of 0.136 eV); while in the case of Pr-doped rutile TiO_2, there is a impurity energy level above the valence band with a distance of 0.308 eV from the VBM (with a bandwidth of 0.092 eV), at the same time, there is an another impurity energy level below the conduction band with a distance of 0.266 eV from the CBM (with a bandwidth of 0.037 eV). The information about bonding mechanism could be provided by the local partial density of states. For both crystal phases (anatase and rutile), the top of valence band is mainly dominated by the characteristics of O-2p non-bonding states, while the bottom of conduction band is mainly dominated by the characteristics of Ti-3d non-bonding states. Importantly, the Pr-4f states (spin up states) hybridized with the O-2p states (spin up state), forming the impurity energy levels above the valence band; while the impurity energy level below the conduction band is predominately composed by the Pr-4f states (spin up states) in the case of Pr-doped rutile TiO_2. And other Pr-related impurity energy levels are mainly located at the energy range of -5~0 eV to contribute the formation of valence band, and located at the energy range of 3-5 eV to contribute the formation of the bottom of conduction band.

Combined with the experimental measurements and theoretical calculations, we could better understand above observations. First, the ability of a photocatalyst to undergo photo-generated electrons transfer to adsorbed species on its surface is governed by the band energy position of the semiconductor and the redox potentials of the adsorbate. The relevant potential level of the acceptor is thermodynamically

required to be below (more positive than) the conduction band potential of photocatalyst. The potential level of the donor needs to be above (more negative than) the valence band position of photocatalyst [46]. For example, for photocatalytic water splitting, a suitable photocatalyst material requires that its CBM energy is higher than the reduction potential of H^+/H_2 and its VBM energy lower than the oxidation potential of O_2/H_2O, in addition to its band gap exceed the incident photon energy. This condition guarantees the photo-generated electrons can take part in the reduction reaction, and the photo-generated holes can take part in the oxidation reaction.[47] So, we calculated the band edge position of TiO_2 according to the methods defined in Ref.[48-51], as shown in FIG. 6. The rough CBM potential of anatase TiO_2 is -0.303 eV with respect to the normal hydrogen electrode. Subsequently the rough VBM potential of anatase TiO_2 is determined as 2.893 eV based on its calculated band gap, which is very consistent with the band energy position of anatase TiO_2 in Ref.[46]. For rutile TiO_2, the VBM potential is up-shifting about 0.668 eV, while the CBM potential is up-shifting about 0.468 eV, in compared with anatase TiO_2. This result indicates that the oxidation ability of photo-generated hole in anatase TiO_2 is higher than that of in rutile TiO_2. By Pr doping, the VBM potential is slightly up-shifting about 0.086 eV, while the CBM potential is slightly up-shifting about 0.020 eV, in compared with pure anatase TiO_2; and the VBM potential is slightly up-shifting about 0.107 eV, while the CBM potential is slightly up-shifting about 0.102 eV, in compared with pure rutile TiO_2. This result suggests that the redox ability of TiO_2 has no obvious impact by Pr doping, so the photocatalytic ability of Pr-doped anatase TiO_2 is still higher than that of Pr-doped rutile TiO_2, as shown in FIG. 4. Second, for the doping modification method, the shallow impurity energy band could act as the capture center of photo-generated carriers.[25] In both cases of anatase and rutile TiO_2, Pr doping induces an impurity energy band above the top of VB, which can capture the photo-generated holes resulting in suppress the recombination rate of photo-generated electron-hole pairs. Therefore, the photocatalytic activity of TiO_2 is enhanced by Pr doping, as shown in FIG. 4. Furthermore, there is an another impurity energy band below the bottom of CB in the case of Pr-doped rutile TiO_2, which can capture the photo-generated electrons, resulting in further suppress the recombination rate of photo-generated electron-hole pairs. This result could explain why the modification effect of Pr is more obvious for rutile TiO_2 than that for anatase TiO_2.

4. Conclusions

In summary, a series of Pr-doped TiO_2 samples with anatase and rutile phases were synthesized by sol-gel method and were systematically characterized. Pr doping does not obviously change the crystal structure and optical absorption of TiO_2, and enhance the photocatalytic activity in the present work. For anatase TiO_2, Pr doping induces a shallow acceptor energy band above the top of valence band; while for rutile TiO_2, Pr doping induces a shallow acceptor energy band above the top of valence band and a shallow donor energy band below the bottom of conduction band. These shallow energy bands could act as the capture center for photo-generated carriers, resulting in suppress the recombination rate of photo-generated electron-hole pairs. Furthermore, in the case of Pr-doped rutile TiO_2, Pr doping induces not only shallow acceptor energy band but also donor energy band; thus, its modification impact for photocatalytic activity is more obvious than that of Pr-doped anatase TiO_2. In the present work, the experimental observations were well confirmed and explained by the theoretical calculations. These observations clarify some unclear issues, and provide guidance for research and applications of ions doping to improve the photocatalytic performance in the future.

Acknowledgments

The authors would like to acknowledge financial support from the National Natural Science Foundation of China (Grant No.21263006).

References

1. D. M. Schultz and T. P. Yoon, *Science*, 2014, **343**, 1239176.
2. J. R. Swierk and T. E. Mallouk, *Chem. Soc. Rev.*, 2013, **42**, 2357.
3. N. Serpone and A. V. Emeline, *J. Phys. Chem. Lett.*, 2012, **3**, 673.
4. M. A. Henderson, *Surf. Sci. Rep.*, 2011, **66**, 185.
5. F. Bonaccorso, L. Colombo, G. Yu, M. Stoller, V. Tozzini, A. C. Ferrari, R. S. Ruoff and V. Pellegrini, *Science*, 2015, **347**, DOI: 10.1126/science.1246501.
6. L. R. Merte, R. Bechstein, G. Peng, F. Rieboldt, C. A. Farberow, H. Zeuthen, J. Knudsen, E. Lægsgaard, S. Wendt, M. Mavrikakis and F. Besenbacher, *Nat Commun*, 2014, **5**.
7. T. Ohno, M. Akiyoshi, T. Umebayashi, K. Asai, T. Mitsui and M. Matsumura, *Appl. Catal. A*, 2004, **265**, 115.
8. M. Harb, P. Sautet and P. Raybaud, *J. Phys. Chem. C*, 2013, **117**, 8892.
9. T. Umebayashi, T. Yamaki, H. Itoh and K. Asai, *Appl. Phys. Lett.*, 2002, **81**, 454.

10. U. Diebold, *Surf. Sci. Rep.*, 2003, **48**, 53.
11. Y. Qu and X. Duan, *Chem. Soc. Rev.*, 2013, **42**, 2568.
12. J. Schneider, M. Matsuoka, M. Takeuchi, J. Zhang, Y. Horiuchi, M. Anpo and D. W. Bahnemann, *Chem. Rev.*, 2014, **114**, 9919.
13. Y. Sakata, T. Yamamoto, T. Okazaki, H. Imamura and S. Tsuchiya, *Chem. Lett.*, 1998, 1253.
14. T. Umebayashi, T. Yamaki, S. Yamamoto, A. Miyashita, S. Tanaka, T. Sumita and K. Asai, *J. Appl. Phys.*, 2003, **93**, 5156.
15. J. Liqiang, S. Xiaojun, X. Baifu, W. Baiqi, C. Weimin and F. Honggang, *J. Solid State Chem.*, 2004, **177**, 3375.
16. E. Sanchez, T. Lopez, R. Gomez, A. Morales and O. Novaro, *J. Solid State Chem.*, 1996, **122**, 309.
17. K. Hiehata, A. Sasahara and H. Onishi, *Nanotechnology*, 2007, **18**, 084007.
18. B. O'regan and M. Grfitzeli, *Nature*, 1991, **353**, 737.
19. F. Chen, Z. Deng, X. Li, J. Zhang and J. Zhao, *Chem. Phys. Lett.*, 2005, **415**, 85.
20. D. Liu and P. V. Kamat, *J. Phys. Chem.*, 1993, **97**, 10769.
21. V. Sukharev and R. Kershaw, *J. Photoch. Photobio. A*, 1996, **98**, 165.
22. Z. Zhang and J. T. Yates, *Chem. Rev.*, 2012, **112**, 5520.
23. X. Chen and S. S. Mao, *Chem. Rev.*, 2007, **107**, 2891.
24. K. Singh, J. Nowotny and V. Thangadurai, *Chem. Soc. Rev.*, 2013, **42**, 1961.
25. R. Asahi, T. Morikawa, T. Ohwaki, K. Aoki and Y. Taga, *Science*, 2001, **293**, 269.
26. B. Leedahl, D. A. Zatsepin, D. W. Boukhvalov, E. Z. Kurmaev, R. J. Green, I. S. Zhidkov, S. S. Kim, L. Cui, N. V. Gavrilov, S. O. Cholakh and A. Moewes, *J. Phys. Chem. C*, 2014, **118**, 28143.
27. F. Da Pieve, S. Di Matteo, T. Rangel, M. Giantomassi, D. Lamoen, G. M. Rignanese and X. Gonze, *Phys. Rev. Lett.*, 2013, **110**, 136402.
28. W.-J. Yin, S.-H. Wei, M. M. Al-Jassim and Y. Yan, *Phys. Rev. Lett.*, 2011, **106**, 066801.
29. K. Yang, Y. Dai, B. Huang and M.-H. Whangbo, *J. Phys. Chem. C*, 2009, **113**, 2624.
30. J. Wang, H. Sun, J. Huang, Q. Li and J. Yang, *J. Phys. Chem. C*, 2014, **118**, 7451.
31. M. Niu, D. Cheng and D. Cao, *J. Phys. Chem. C*, 2013, **117**, 15911.
32. N. Feng, Q. Wang, A. Zheng, Z. Zhang, J. Fan, S.-B. Liu, J.-P. Amoureux and F. Deng, *J. Am. Chem. Soc.*, 2013, **135**, 1607.
33. F. P. Huang, Y. G. Fan and J. J. Sun, *Advanced Materials Research*, 2012, **557**, 497.
34. J. Wu, Q. Liu, P. Gao and Z. Zhu, *Mater. Res. Bull.*, 2011, **46**, 1997.
35. A.-W. Xu, Y. Gao and H.-Q. Liu, *J. Catal.*, 2002, **207**, 151.
36. Z. Zhao and Q. Liu, *J. Phys. D. Appl. Phys.*, 2008, **41**, 085417.
37. S. J. Clark, M. D. Segall, C. J. Pickard, P. J. Hasnip, M. J. Probert, K. Refson and M. C. Payne, *Z. Kristallogr.*, 2005, **220**, 567.
38. J. P. Perdew, A. Ruzsinszky, G. I. Csonka, O. A. Vydrov, G. E. Scuseria, L. A. Constantin, X. Zhou and K. Burke, *Phys. Rev. Lett.*, 2008, **100**, 136406.
39. V. I. Anisimov, J. Zaanen and O. K. Andersen, *Phys. Rev. B*, 1991, **44**, 943.
40. B. G. Pfrommer, M. Câté, S. G. Louie and M. L. Cohen, *J. Comput. Phys.*, 1997, **131**, 233.
41. C. Gao, H. Song, L. Hu, G. Pan, R. Qin, F. Wang, Q. Dai, L. Fan, L. Liu and H. Liu, *J. Lumin.*, 2008, **128**, 559.
42. Y. Ma, J. Zhang, B. Tian, F. Chen and L. Wang, *J. Hazard. Mater.*, 2010, **182**, 386.
43. Q. Xiao, L. Ouyang, L. Gao and W. Jiang, *Mater. Chem. Phys.*, 2010, **124**, 1210.
44. J. K. Burdett, T. Hughbanks, G. J. Miller, J. W. Richardson and J. V. Smith, *J. Am. Chem.*

Soc., 1987, **109**, 3639.

45. C. G. Van de Walle and J. Neugebauer, *J. Appl. Phys.*, 2004, **95**, 3851.
46. A. L. Linsebigler, G. Lu and J. T. Yates, *Chem. Rev.*, 1995, **95**, 735.
47. A. Kudo and Y. Miseki, *Chem. Soc. Rev.*, 2009, **38**, 253.
48. S.-H. Wei and A. Zunger, *J. Appl. Phys.*, 1995, **78**, 3846.
49. S. Chen, A. Walsh, J.-H. Yang, X. G. Gong, L. Sun, P.-X. Yang, J.-H. Chu and S.-H. Wei, *Phys. Rev. B*, 2011, **83**, 125201.
50. M. A. Butler and D. S. Ginley, *J. Electrochem. Soc.*, 1978, **125**, 228.
51. Y. Xu and M. A. A. Schoonen, *Am. Mineral.*, 2000, **85**, 543.

TABLE 1. The lattice distortion and the impurity formation energy of Pr-doped TiO_2; and the average atomic or bond populations of pure TiO_2 and Pr-doped TiO_2 by Mulliken analysis

Models	E_f /eV	Bond Length /Å		ΔV /Å^3	Atomic or Bond Population /e				
		Ti-O	Pr-O		Ti	Pr	O	Ti-O	Pr-O
Pure anatase TiO_2		1.9309, 1.9861			1.290		-0.640	0.750, 0.250	
Pr-doped anatase TiO_2	1.68	1.9291, 1.9972	2.1147, 2.2170	0.630	1.262	1.720	-0.636	0.385, 0.279	0.220, 0.110
Pure rutile TiO_2		1.9456, 1.9785			1.240		-0.620	0.780, 0.260	
Pr-doped rutile TiO_2	2.10	1.9326, 1.9731	2.1588, 2.1711	0.997	1.210	1.730	-0.617	0.416, 0.420	0.320, 0.270

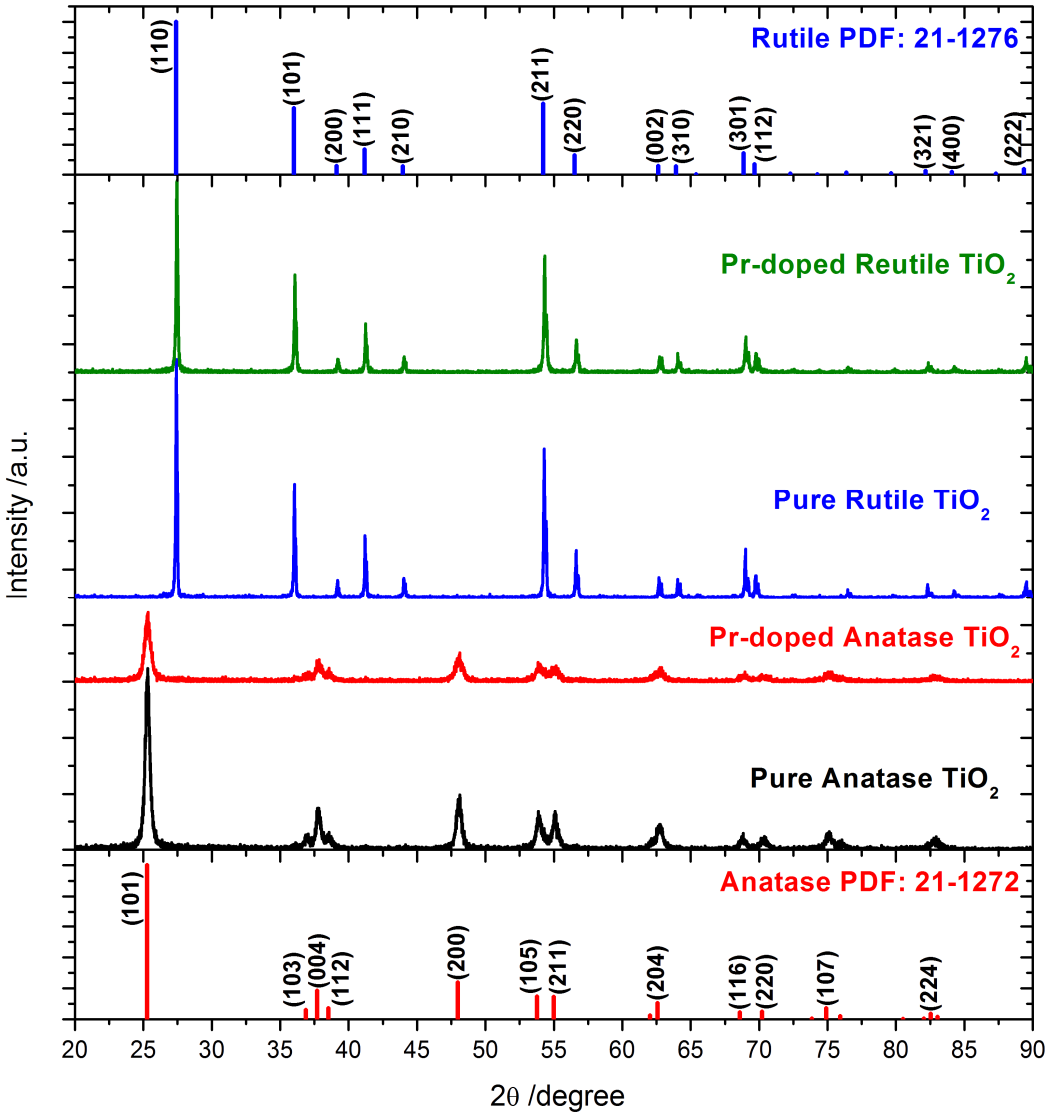

FIG. 1 The XRD patters of pure TiO_2 and Pr-doped TiO_2

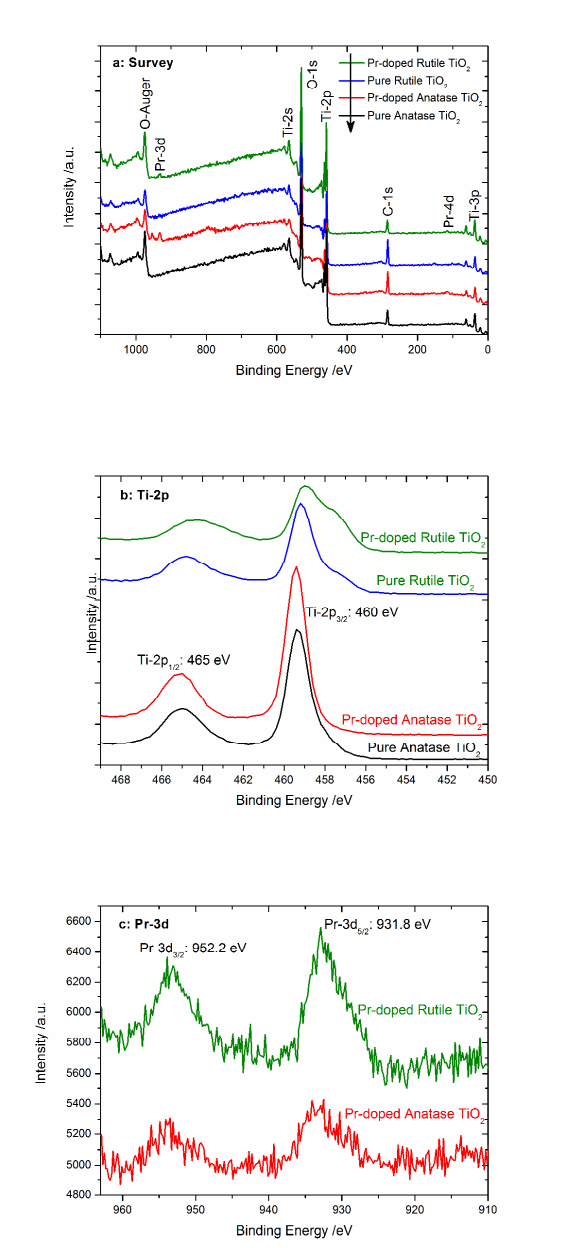

FIG. 2 The XPS measurement for pure TiO_2 and Pr-doped TiO_2

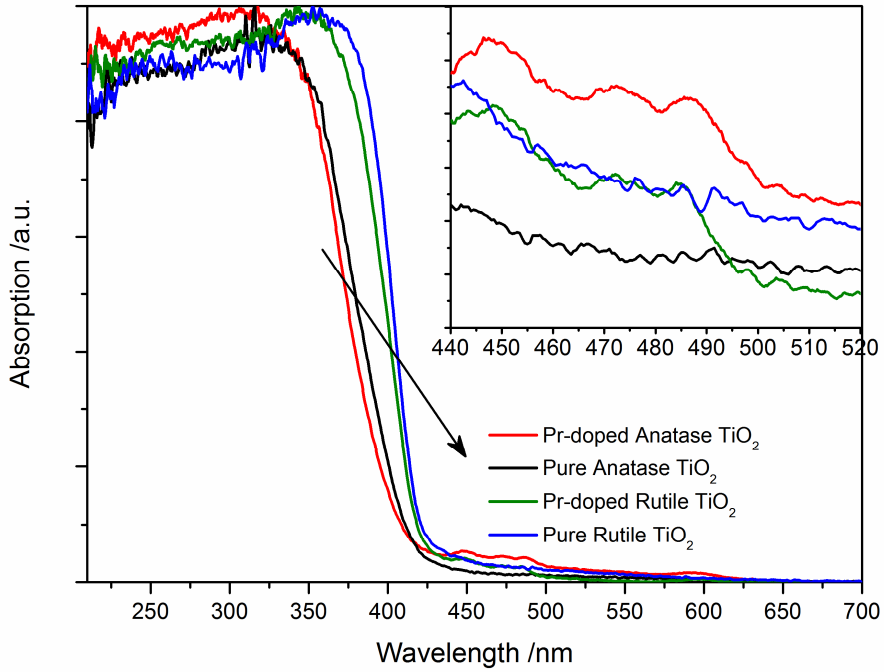

FIG. 3 The UV-Vis absorption spectra of pure TiO_2 and Pr-doped TiO_2

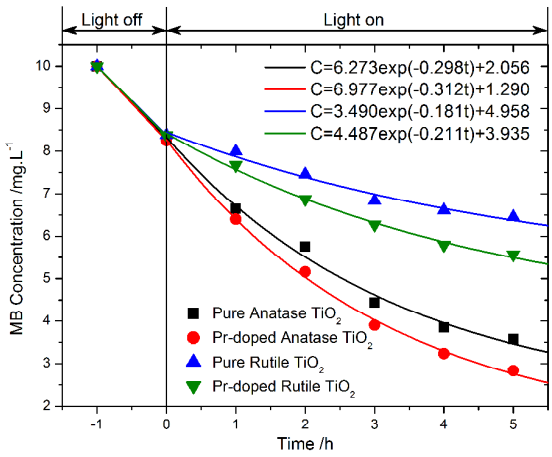

(a)

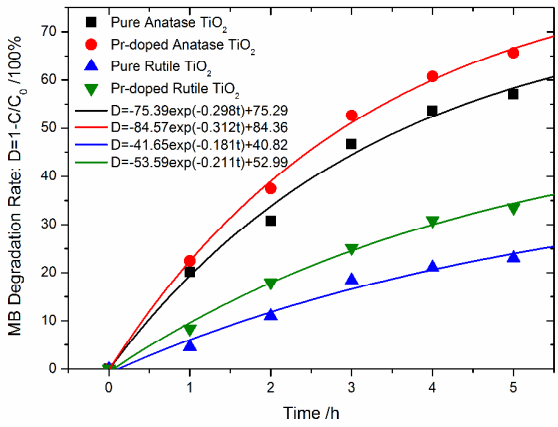

(b)

FIG. 4 The MB concentrations and photocatalytic degradation rate as function of time in pure TiO_2 and Pr-doped TiO_2

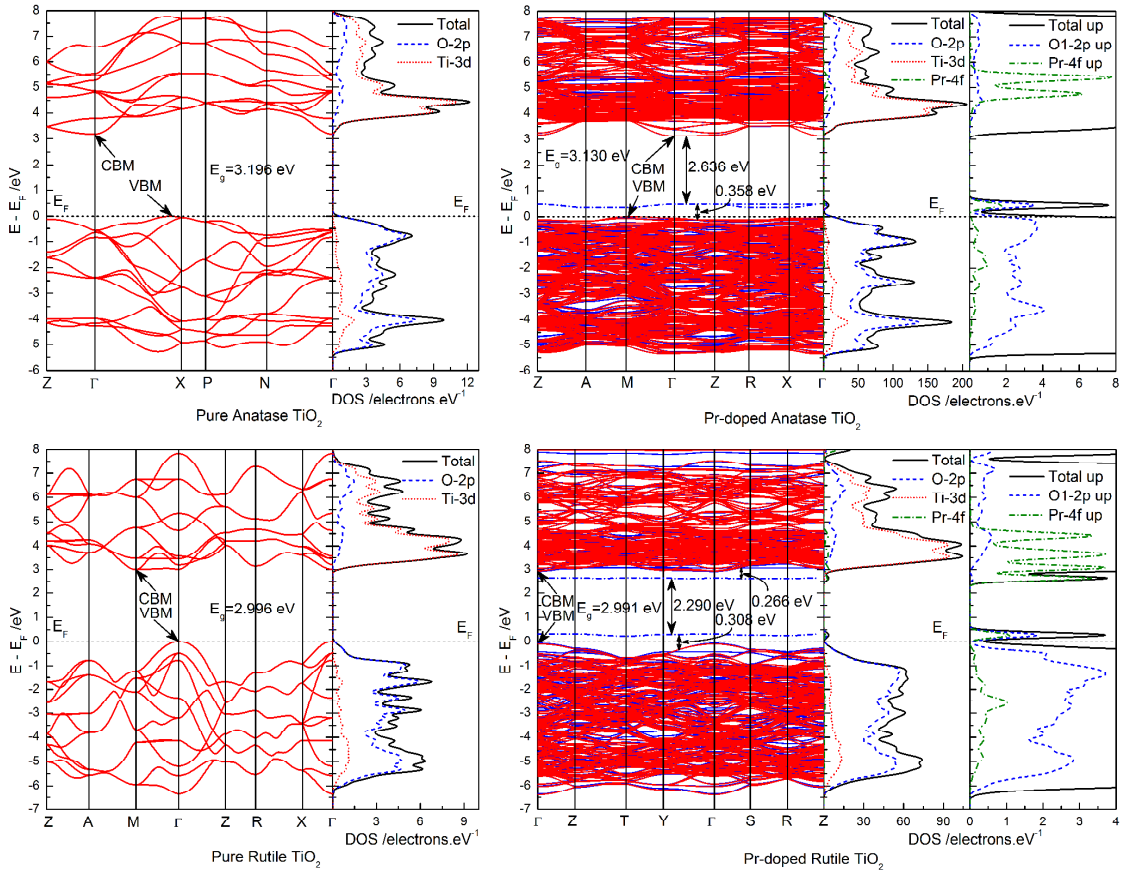

FIG. 5 The DFT calculated band structure and density of states of pure TiO_2 and Pr-doped TiO_2, the blue lines represent the spin-down states, and the red lines represent the spin-up states.

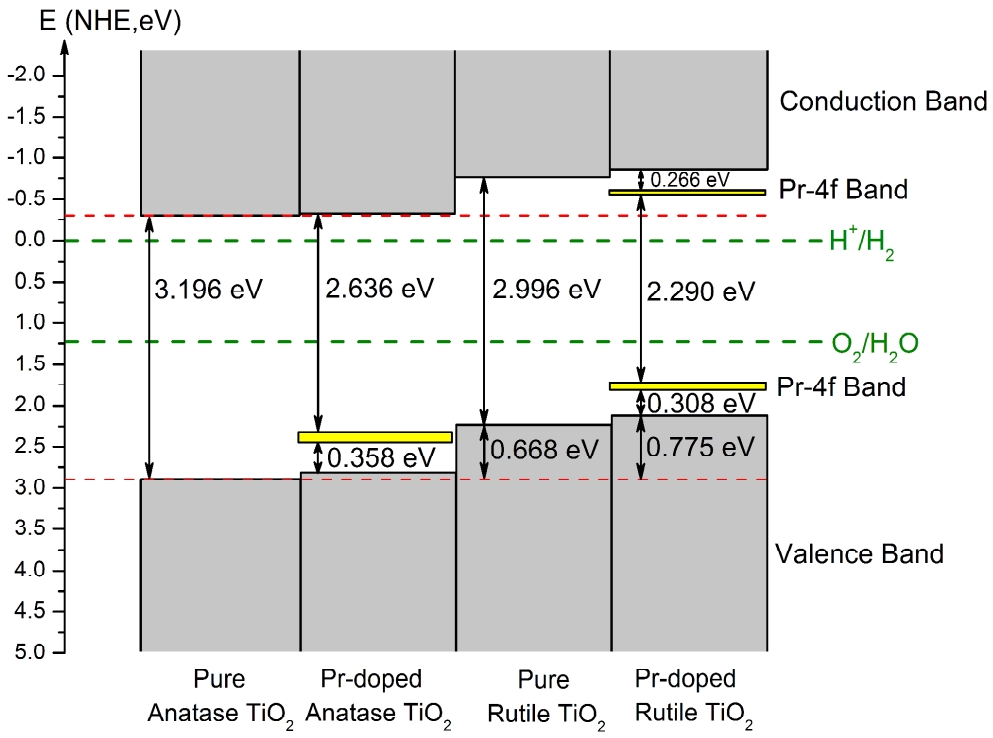

FIG. 6 The band edge alignment of pure TiO_2 and Pr-doped TiO_2